Research Paper

Behavior of an embankment on soft deposit improved by column-link method

J.C. Chai [1], J. Ni [2*] and M.D. Liu [3]

ARTICLE INFORMATION

ABSTRACT

The behavior of a test embankment on soft deposit improved by column-link method in Saga, Japan, was investigated by three dimensional (3D) finite element analysis (FEA). In column-link method, the column-walls under the shoulders of an embankment are linked by geogrids or cables to restrict lateral movement of the walls and partially reduce the embankment settlement. A geogrid with a tensile strength of 36 kN/m and yielding strain of 12% was used and relatively large lateral displacement of about 0.18 m occurred. The results of FEA showed that the geogrid might yield. The results indicated that to effectively restrain lateral movement of the walls, geogrids with high tensile strength and stiffness, like steel cables were needed. With the conditions of the test embankment, using steel cables, the mobilized tensile force in the cable could reach more than 600 kN/m. Further, at the upper part of the column walls, high compression or tensile stresses could be developed with strong linking geogrids. Thus, reinforcing the column walls with steel bar or H-steel is required. The results from this study showed a properly designed column-link method could be an effective and economic soft ground improvement method.

1. Introduction

Soft soil deposit normally has high water content, high compressibility and low shear strength. When constructing an earth structure on a soft deposit, some kinds of ground improvements are usually needed. Deep cement mixing (DCM) normally forming soil-cement columns in the deposit is one of the widely used methods in engineering practice (Han et al., 2012; Bergado et al., 2008; Liu et al., 2007; Liu et al., 2012; Onur and balaban, 2018; Chai et al., 2015; Chai et al., 2013).

To reduce construction cost, a method called column-link has been developed. **Figure 1** illustrates the column-

link method. The method improves the soft deposit using columns with different length. The inner zone is improved by floating (shorter) columns while the outer zones are improved by end-bearing columns. Between the inner and outer zones, column walls penetrated into a stiffer soil layer are constructed, and the heads of two walls are linked by steel cables or geogrids. H-steel beams can be inserted into the column-walls to increase its bending resistance if necessary. This method has been developed in Japan and had some applications (Matsui et al., 2013; Kondoh and Miyatake, 2018), while there are still some issues need to be investigated regarding the performance of the system, such as the requirement for the cables of

[1] Professor, Faculty of Science and Engineering, Saga University, 1 Honjo, Saga 840-8502, JAPAN, chai@cc.saga-u.ac.jp
[2*] Corresponding author, PhD Candidate, Faculty of Science and Engineering, Saga University, 1 Honjo, Saga 840-8502, JAPAN, nijunfeng007@163.com
[3] Department of Civil, Mining and Environmental Engineering, University of Wollongong, NSW 2522, AUSTRALIA, martindl@uow.edu.au
Note: Discussion on this paper is open until September 2020

280

Chai et al. / Lowland Technology International 2020; 21 (4): 279-286
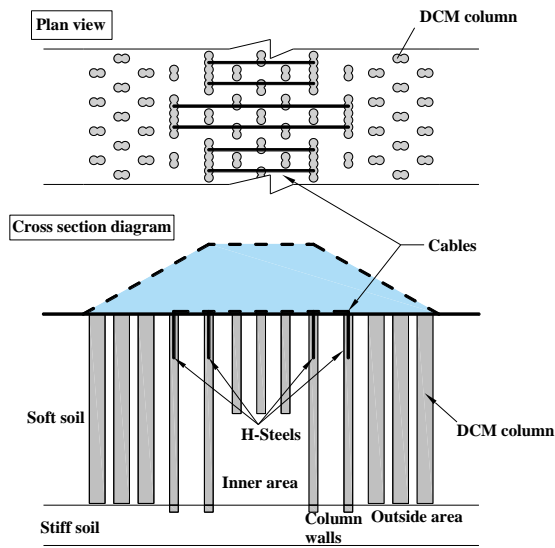**Special Issue on: Engineering Geology and Geotechniques for Developing Countries**

Fig. 1. Sketch of column-link method

geogrids to link the column walls, possible bending moment developed in the wall under an embankment load, etc.

A test embankment was constructed on a soft clay deposit improved by the column-link method in Saga, Japan. In this study, the test embankment was simulated by three dimensional (3D) finite element analysis (FEA) to investigate the effect of the strength and stiffness of the cable or geogrid on the performance of the system and the stress distribution in the column walls. The site condition, the embankment construction and the field monitoring system are presented firstly. Then the filed measured and simulated results are compared in terms of settlements, lateral displacements and pore pressures. Finally, the results of numerical investigation are presented and discussed, and the suggestions for designing the column-link system are provided.

2. Subsoil profile and ground improvement

2.1 Subsoil profile

At the site, the soil layers had a thickness of 21.9 m. From the ground surface, there is a silty clay layer of 2.9 m in thickness. Below it is a clayey sand layer of 2.8 m. Under the clayey sand layer is a silty clay layer of 16.2 m in thickness underlain with a gravelly sand layer. Some of physical and mechanical properties of the subsoils are summarized in **Fig. 2**. The ground water level was 0.52 m depth from the ground surface, at the time of the site investigation.

2.2 Construction of soil-cement column

The soil-cement columns were constructed by a double axes machine, i.e. two columns can be constructed at once. The diameter of a column was 1.0 m, and spacing between two columns was 0.8 m (center-to center). There are some overlapping of the two columns. The amount of cement used was 150 kg/m^3 and designed unconfined compressive strength, q_u, was 1000 kPa. The plan layout of the columns is shown in **Fig. 3**. The length of the columns varied from 11.4 m (center areas) to 22.7 m (column-wall). The average area improvement ratio was approximately 15.5%.
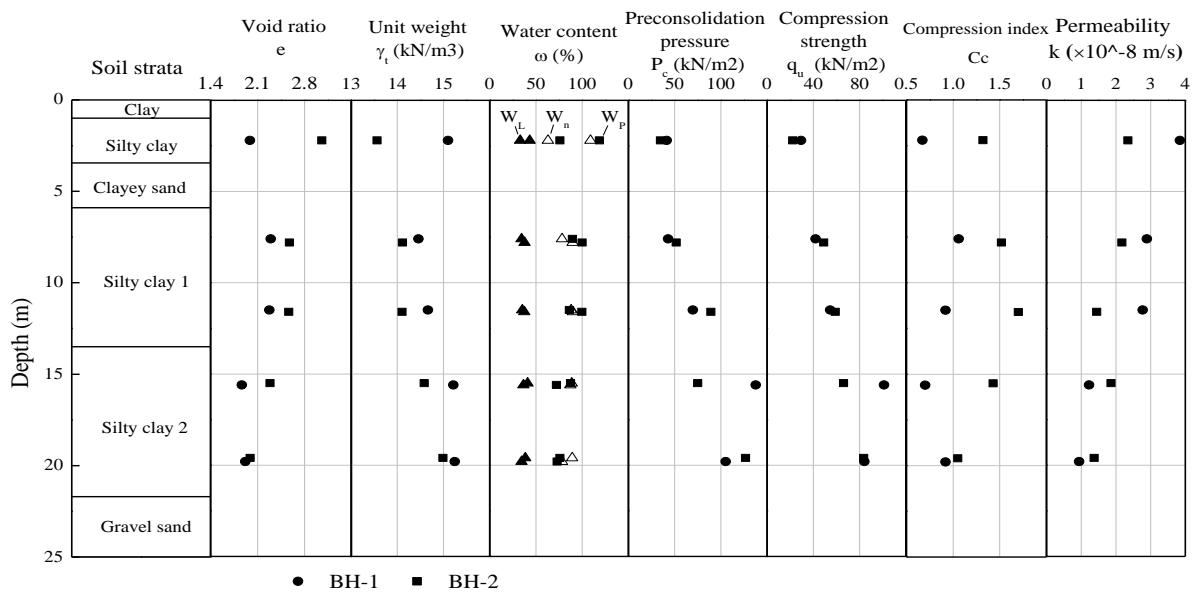
2.3 Geogrids used

Fig. 2. Soil profile and some engineering properties of soils at the site.

281

Chai et al. / Lowland Technology International 2020; 21 (4): 279-286
Special Issue on: Engineering Geology and Geotechniques for Developing Countries

A geogrid used was made of polyester fiber for the longitudinal strips, while the transverse ribs composed of aramid fiber with a low tensile strength. Based on the information from the manufacturer, tensile strength in short
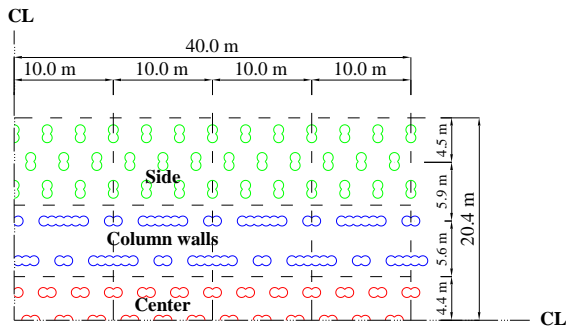

Fig. 3. Plan layout of the columns

term is 50 kN/m with a failure strain of approximately 12%. The suggested tensile strength considering creep is 36 kN/m. Since the strength of geogrid in transverse diction was low, two layers of geogrid were laid at the base of the embankment perpendicular to each other, which covered the entire base area of the embankment.

2.4 Embankment construction and field monitoring

The embankment had a fill thickness of 8.0 m and side slope 1:1.8 (V:H). The base dimension was 40.8 m by 78.8 m and the final top dimension was 12 m by 50 m. The fill used was decomposed granite and compacted fill had a unit weight of approximately 20 kN/ m^3. The embankment was constructed step by step with an average filling rate of around 0.05 m/day and the total construction time was 151 days.
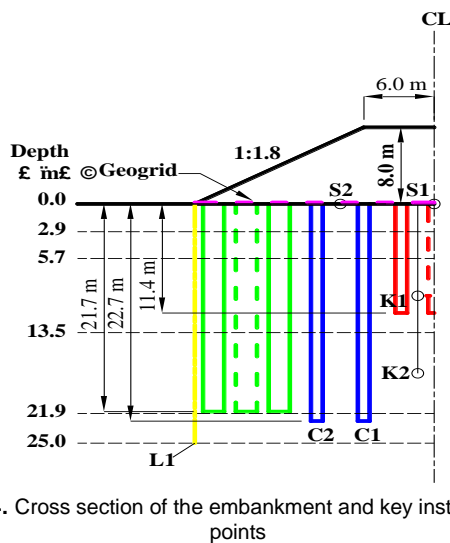

Fig. 4. Cross section of the embankment and key instrument points

The embankment cross-section and some key field monitoring points are shown in **Fig. 4**. S1 and S2 are surface settlements points. L1 is inclinometer casing and

K1 and K2 are excess pore water pressure gauges. The monitoring started at the beginning of embankment construction and lasted for 952 days.

3. Finite Element Simulation

3.1 Finite element modeling

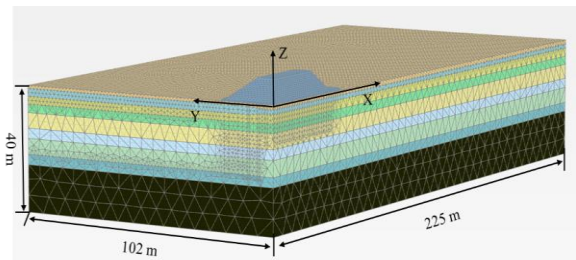3D finite element simulation was performed by Plaxis

Fig. 5. Meshed 3D model of the embankment

3D (2018 version). Ten-node cubic elements were used for soils and sheet elements were adopted for geogrids. Due to the symmetry, only a quarter of the embankment was modelled, as shown in **Fig. 5**. The modeled volume was 225 m long, 102 m wide and 40 m in depth from the ground surface. The total number of elements used was about 190,000 and the total number of nodes was about 250,000.

For the displacement boundary conditions, the bottom was fully fixed but the top was free. At the vertical boundaries perpendicular to x- or y-axis, the displacement normal to the boundaries was fixed. For the hydraulic boundary conditions, all the horizontal boundaries were set as impermeable while the top and bottom boundaries were permeable.

The single column was a cylinder in the field, for easy meshing, the columns were modeled as rectangular prisms according to equal bending rigidity (*EI*, *E* is Young's modulus and *I* is moment of inertia of the cross section area) condition. The cross sections of converted columns are rectangles with 1.68 m × 0.88 m for two-columns connected type and 4.98 m × 0.88 m for six-columns connected type.

In FEA simulation, clay soil layers were modelled by soft soil model (SSM), while clayey gravel and sand layer were simulated by Mohr-Coulomb (MC) model. The columns and embankment fill material were also modelled with MC model. Between columns and surrounding soils, joint elements were used. The geogrid was modeled as a linear elastic-perfect plastic material.

The construction process for embankment was divided into 14 phases. The fill thickness was 0.3 m for phase 1-2, but 0.6 m for phases 3-13, and 0.8 m for the final phase. In addition, updating nodal coordinates option was

282

Chai et al. / Lowland Technology International 2020; 21 (4): 279-286
Special Issue on: Engineering Geology and Geotechniques for Developing Countries

Table 1. The parameters adopted in the simulation

Depth (m)	Soil strata	E (kPa)	v	c' (kPa)	ϕ' (°)	λ^*	κ^*	M	e	γ_t (kN/m3)	k_v (10^{-4}m/day)	k_h (10^{-4}m/day)	OCR
0-1.45	Clay	-	0.15	8	30	0.145	0.029	1.6	1.987	15.1	33.2	49.9	7.0
1.45-2.9	Silty clay	-	0.15	7	30	0.145	0.029	1.6	1.987	15.1	33.2	49.9	2.5
2.9-5.7	Silty sand	-	0.15	8	30	0.145	0.029	1.6	1.987	15.1	33.2	49.9	1.5
5.7-9.7	Silty clay-1-1	-	0.15	6	30	0.200	0.04	1.6	2.576	14.1	18.8	28.2	1.0
9.7-13.45	Silty clay-1-2	-	0.15	6	30	0.226	0.045	1.6	2.566	14.1	12.5	18.7	1.0
13.45-17.7	Silty clay-2-1	-	0.15	8	30	0.189	0.038	1.6	2.285	14.6	16.1	24.1	1.2
17.7-21.9	Silty clay-2-2	-	0.15	6	30	0.137	0.027	1.6	1.916	15.3	11.8	12.2	1.0
21.9-25	Clayey Gravelly	3×10^4	0.1	0	40	-	-	-	0.7	20.0	25.0	25.0	-
25-50	Sand	3×10^4	0.1	0	40	-	-	-	0.7	20.0	250.0	250.0	-
Embankment fill		1000	0.45	10	35	-	-	-	0.8	20.0	-	-	-
Columns		15×10^4	0.1	750	0	-	-	-	same with surrounding soil				-

adopted at the end of each phase considering large deformation phenomenon.

3.2 Modeling parameters.

The model parameters adopted are listed in **Table 1**. For soil layers, the vertical permeability (k_v), void ratio (e), unit weight (γ), over-consolidation ratio (OCR), λ^* ($\lambda^* = \lambda(1+e_0)$, λ is the slope of virgin compression line in e-lnp' plot), are measured values from laboratory tests. The values of κ^* ($\kappa^* = \kappa/(1+e_0)$) was assumed to be 1/10 of λ^*. The horizontal permeability k_h was assumed to be equal to vertical permeability k_v in sands and clayey gravels, but 1.5 times k_v for clay soils. The values of permeability are initial ones. During consolidation process, permeabilities varied with void ratio according to Taylor (1948) equation,

$$k = k_0 \cdot 10^{(e-e_0)/C_k} \qquad [1]$$

where e_0 is initial void ratio, k_0 is the initial permeability, and C_k is a constant. The adopted C_k value was $0.5e_0$ (Tavenas et al. 1983). Effective stress friction angles were assumed. The values of effective cohesive were evaluated by comparing the measured unconfined compressive strength and the undrained shear strength predicted by SSM (Chai et al., 2017a). The M values were assumed to be 1.6 for all soft soils (Chai et al., 2013; Chai et al., 2017b). The Poisson's ratios (v) were assumed to be 0.15 and 0.1 for clay soils and sands and gravels, respectively.

The designed unconfined compressive strength q_u for the columns was 1000 kPa. However, the simulation results showed that with q_u for the columns of 1500 kPa gave a better agreement with the measured data. Thus, q_u

of 1500 kPa was adopted for the columns. The void ratio, unit weight and permeability of the columns were assumed to be the same as the surrounding soils. The Young's modulus, E, was evaluated to be 100 times q_u. The tensile strength σ_t was set as $q_u/10$ (Porbaha et al., 2000; Chai et al., 2018). The effective cohesion c' was estimated to be 1/2 of q_u, by assuming the effective stress internal friction angle ϕ' of zero. The Poisson's ratio (v) was assumed to be 0.1 (Chai et al., 2010).

The Young's modulus E of the embankment fill was assumed to be 1000 kPa and Poisson's ratio (v) was assumed to be 0.45 (Chai et al., 2017a). The values of c' and ϕ' were assumed to be 10 an d 35° respectively.

The mechanical behavior of the joint element was simulated using elastic-perfectly plastic model. The interface shear strength was assumed the same as that of the surrounding soil. The shear modulus of the interface (G_i) is calculated as,

$$G_i = \frac{(1+e_0)\sigma'_n}{\lambda} \cdot \frac{3(1-2v_i)}{2(1+v_i)} \qquad [2]$$

where σ'_n is the normal stress on the interface. Parameter v_i is the Poisson's ratio, and a value of 0.45 was adopted, which simulated a close to undrained shearing. To calculate the interface shear stiffness, an imaginary thickness of the joint element is needed, and a value of 0.1 m was adopted.

3.3 Strength and stiffness of geogrids and the cases analysis.

Three cases were analyzed as listed in **Table 2**. The tensile strength and stiffness of geogrids adopted for Case

283

Chai et al. / Lowland Technology International 2020; 21 (4): 279-286
Special Issue on: Engineering Geology and Geotechniques for Developing Countries

Table 2. Mechanical properties of geogrids for the cases analyzed

Case	Yielding strain (%)	Tensile strength (kN/m)	Normal stiffness, EA (kN/m)	Remark
1	12	36	300	Simulate actual case
2	5	144	2880	Assumed case
3	0.22	650	295454	Assumed case

(a) Cases 1 and 2
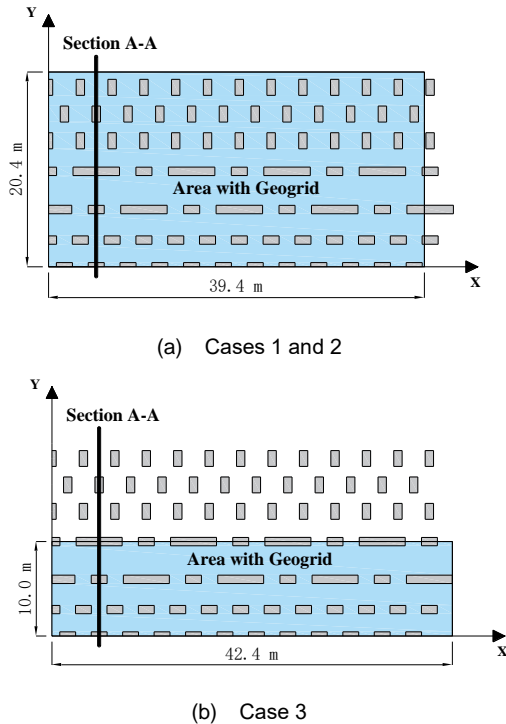
(b) Case 3

Fig. 6. Layouts of geogrids at the base of the embankment

1 simulated the field case, and Case 2 and 3 were assumed. Areas of the base of embankment with geogrid are illustrated in **Fig. 6**. The linking material considered for Case 3 is steel cables. Adopting a tensile strength of steel of 450 N/mm^2, Case 3 requests 6 steel cables with 16 mm in diameter each per meter width.

It was assumed that per meter width, two H-steels were inserted into the column walls up to 5 m depth from the ground surface. Each H-steel had a moment of inertia (I) of 8.7×10^{-5} m^4 respecting to x-axis, and the Young's modulus (E) of steel is 2×10^8 kPa.

4. Comparison of measured and simulated results

4.1 Settlements

The simulated settlements at S1 and S2 (see **Fig. 4**) are compared with measured data in **Fig. 7** (a) and (b),

respectively. S1 located between columns and under the center of the embankment, where S2 was 8 m away from the center and between two rows of end bearing column walls. It can be seen that the Case 1 resulted in a reasonable simulation of the measured data. With the increase of strength and stiffness of the geogrid, there is an obvious reduction of settlement for Case 3. The reduction of settlements at S1 (between floating columns) is more obvious than at S2.
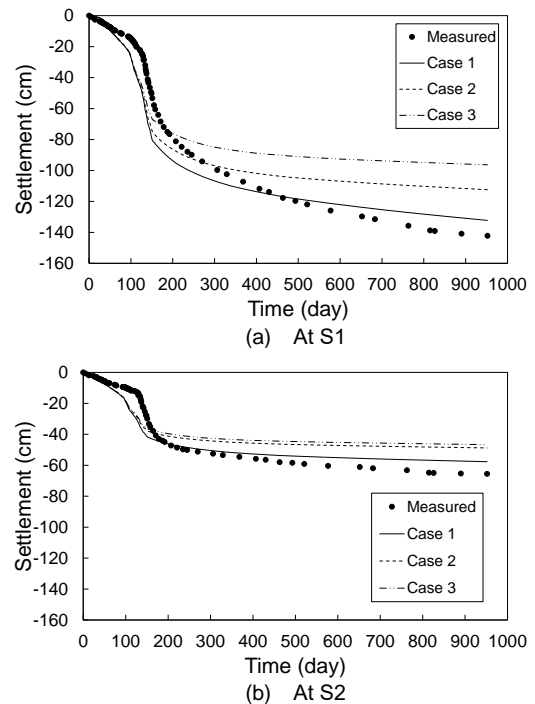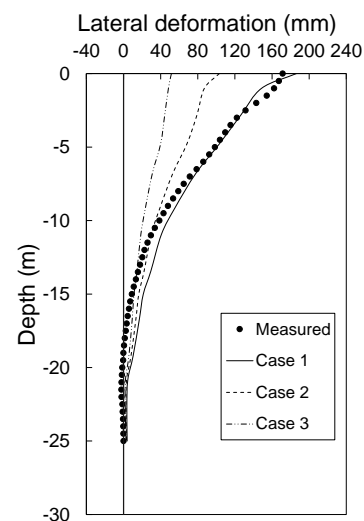
4.2 Lateral displacements

(a) At S1

(b) At S2

Fig. 7. Settlement-time curves

Fig. 8. Lateral displacement profiles at elapsed time of 952 days at L1

284

Chai et al. / Lowland Technology International 2020; 21 (4): 279-286
Special Issue on: Engineering Geology and Geotechniques for Developing Countries

The lateral displacement profiles of the ground under the toe of the embankment at L1 (shown in **Fig. 4**) at the elapsed time of 952 days are compared in **Fig. 8**. Although the simulation (Case 1) over predicted the lateral deformations in most depths, we judge the simulation is fair. The figure also indicates that with the increase the strength and stiffness of the geogrids, the lateral deformation reduced considerably.

4.3 Excess pore water pressures
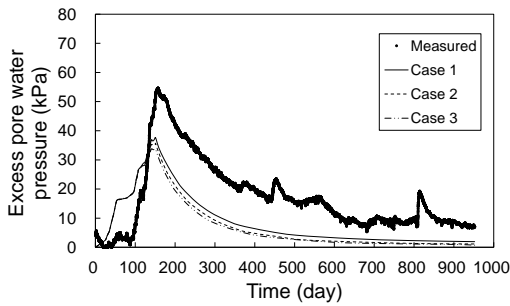
(a)   Excess pore water pressure at point K1
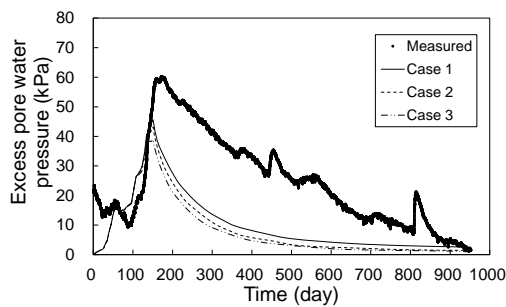
(b)   Excess pore water pressure at point K2

Fig. 9. Variation of excess pore water pressure with elapsed time

The measured and simulated excess pore water pressures at K1 (-9.6 m) and K2 (-17.7 m) in **Fig. 4**, are compared in **Fig. 9**. The simulations are lower than the measured data especially at K2 location. A possible reason is that the adopted permeability of that soil layer might be higher than the actual value.
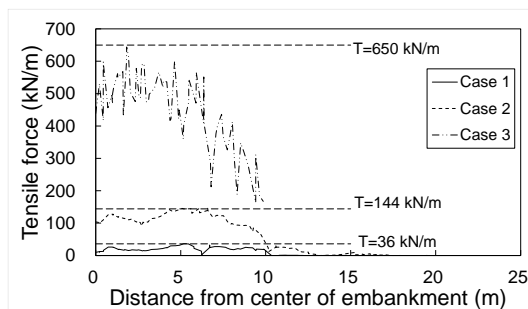

Fig. 10. Tensile force of geogrid with the distance

4.4 Tensile forces in geogrids

The simulated tensile forces in the geogrids along the section A-A (in **Fig. 6**) at elapsed time of 952 days are presented in **Fig. 10**. Section A-A was 5 m away from the center of embankment, where largest tensile forces were simulated.

The simulated tensile forces in the geogrid almost proportionally increased with the increase of the tensile strength and stiffness. The simulated maximum tensile force reached the tensile strength of the geogrids for Case 1 and 2, indicating the yielding of the geogrids. For Case 3, the maximum value is close to 600 kN/m, but still below the tensile strength. This indicates that for designing column-link ground improvement, possible tensile failure of the linking geogrids or steel cables is an important design item.

4.5 Effective vertical stress in column-walls

Tied the column-walls by geogrid or cable will cause bending deformation of the walls. Since the soil-cement columns are weaker in tension, there is a possibility of tensile failure of the walls, and/or the stress concentration on the walls to cause compression failure. The vertical effective stress of inner side (toward embankment center) and outer side of column-walls are checked using FEA results.
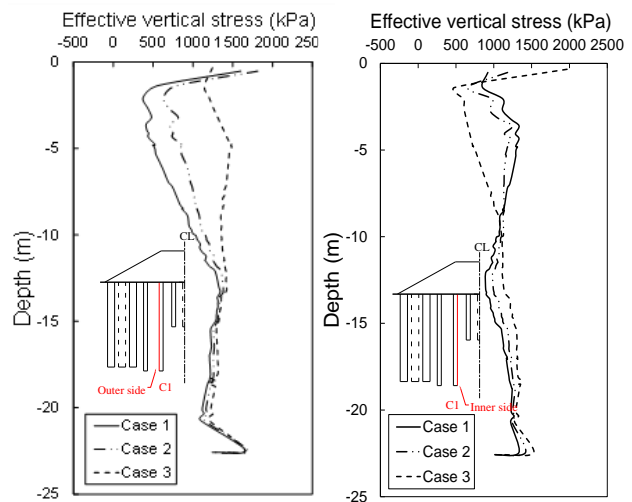

Fig. 11. Variation of effective vertical stress in column-wall

The results for walls C1 and C2 are depicted in **Fig. 11** and **Fig. 12**, respectively. The location of C1 and C2 are illustrated by inserted figures in **Fig. 11** and **Fig. 12**.

For C1 wall, there is no tensile stress developed on both inner and outer sides, but the compression stress in top part of the walls exceed the compression strength of the soil-cement of 1500 kPa at the inner side of the wall for Cases 1 & 2 and the outer side for Case 3. These results

285
Chai et al. / Lowland Technology International 2020; 21 (4): 279-286
Special Issue on: Engineering Geology and Geotechniques for Developing Countries

indicate that even for Cases 1 & 2, the H-steel beam might need to be inserted into the top part of the walls to enhance its strength.

For column-wall C2, there are tensile stress developed at the outer side for Case 3. Since H-steel was inserted into it from ground surface to 5 m depth, which had a high
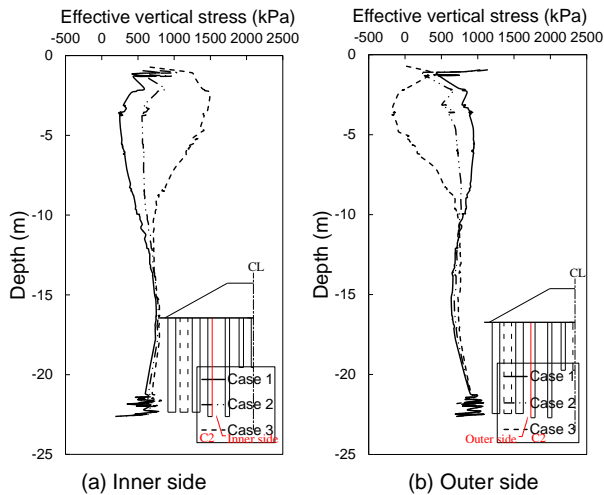

(a) Inner side   (b) Outer side

Fig. 12. Variation of effective vertical stress in column-wall C2

bending resistance. It has been checked that simulated bending moment on the wall is less than the bending resistance of the assumed H-steel along and therefore no bending failure to occur. For Case 3, at the inner side of the wall, the compression stress almost reached the strength of the column. These results implied that Case 3 with high strength and stiffness has a large bending moment in the column-walls, while H-steel can prevent the bending failure.

The results in **Fig. 11** and **Fig. 12** indicate that check the possible bending failure of the top part of the linking column-walls is another important design item of column-link method.

5. Conclusions

The behavior of a test embankment on soft deposit improved by column-link method in Saga, Japan, has been investigated using the results of field measurement and three dimensional (3D) finite element analyses (FEA). In column-link method, soil-cement column walls under the shoulders of an embankment are linked by geogrids or steel cables to restrict their lateral movement and partially reduce the embankment settlement. Based on the field measured and numerically simulated results, following conclusions can be drawn.

(1) A geogrid with a tensile strength of 36 kN/m and yielding strain of 12% was used in the field and relatively large lateral displacement under the toe of the embankment of about 0.18 m was measured. The results of FEA showed that the geogrid might yield.

These results indicate that to effectively restrain lateral movement of the soil-cement walls, a geogrid with high tensile strength and stiffness, like steel cables is needed. For example, with the conditions of the test embankment, using steel cables, the mobilized tensile force in the cables could reach more than 600 kN/m.

(2) The FEA results indicate that when using strong linking geogrids, like steel cables, at the upper part of the column-walls, high compression and/or tensile stresses can be developed in the walls. Thus reinforcing the walls with steel bar or H-steel is required.

(3) The results from this study suggest that column-link method can be an effective and economic soft ground improvement method for embankment construction.

Acknowledgements

References

Bergado, D. T., P. Jamsawang, T. Tanchaisawat, Y. P. Lai, and G. A. Lorenzo. 2008. Performance of reinforced load transfer platforms for embankments supported by deep cement mixing piles. Paper read at GeoCongress 2008: Geosustainability and Geohazard Mitigation, at New Orleans, LA.

Chai, J.-C., S. Shrestha, T. Hino, and T. Uchikoshi. 2017a. Predicting bending failure of CDM columns under embankment loading. Computers and Geotechnics 91:169-178.

Chai, J., J. P. Carter, N. Miura, and H. Zhu. 2010. Improved prediction of lateral deformations due to installation of soil-cement columns. Journal of Geotechnical and Geoenvironmental Engineering 135 (12):1836-1845.

Chai, J., Y. Igaya, T. Hino, and J. Carter. 2013. Finite element simulation of an embankment on soft clay - Case study. Computers and Geotechnics 48:117-126.

Chai, J., Y. Lu, and T. Uchikoshi. 2018. Behavior of an Embankment on Column–Slab Improved Clay Deposit. International Journal of Geosynthetics and Ground Engineering 4 (4).

Chai, J. C., T. Hino, and S. L. Shen. 2017b. Characteristics of clay deposits in Saga Plain, Japan. Proceedings of the Institution of Civil Engineers: Geotechnical Engineering 170 (6):548-558.

Chai, J. C., S. Shrestha, T. Hino, W. Q. Ding, Y. Kamo, and J. Carter. 2015. 2D and 3D analyses of an embankment on clay improved by soil-cement columns. Computers and Geotechnics 68:28-37.

Han, J., A. Bhandari, and F. Wang. 2012. DEM analysis of stresses and deformations of geogrid-reinforced embankments over piles. International Journal of Geomechanics 12 (4):340-350.

Kondoh, M., and H. Miyatake. 2018. A soil improving method capable of controlling peripheral ground displacement. Zairyo/Journal of the Society of Materials Science, Japan 67 (1):18-23.

Liu, H., C. W. Ng, and K. Fei. 2007. Performance of a geogrid-reinforced and pile-supported highway embankment over soft clay: case study. Journal of Geotechnical and Geoenvironmental Engineering 133 (12):1483-1493.

Liu, S., Y. Du, Y. Yi, and A. J. Puppala. 2012. Field Investigations on Performance of T-Shaped Deep Mixed Soil Cement Column-Supported Embankments over Soft Ground. Journal of Geotechnical and Geoenvironmental Engineering 138 (6):718-727.

Matsui, H., H. Ishii, and K. Horikoshi. 2013. Hybrid application of deep mixing columns combined with walls as a soft ground improvement method under embankments. Paper read at 18th International Conference on Soil Mechanics and Geotechnical Engineering: Challenges and Innovations in Geotechnics, ICSMGE 2013.

Onur, M. İ., and E. balaban. 2018. A Numerical Model on Geosynthetic Reinforced Pile Supported Embankments. Anadolu University Journal of Science and Technology-A Applied Sciences and Engineering:484-498.

Porbaha, A., S. Shibuya, and T. Kishida. 2000. State of the art in deep mixing technology. Part III: Geomaterial characterization. Ground Improvement 4 (3):91-110.

Tavenas, F., P. Jean, P. Leblond, and S. Leroueil. 1983. The permeability of natural soft clays. Part II: permeability characteristics. Canadian Geotechnical Journal 20 (4):645-660.

Taylor, D. W. 1948. Fundamentals of soil mechanics. John Wiley and Sons New York.

Symbols and abbreviations

FEA	Finite Element Analysis
OCR	Over-consolidation ratio